Benefits of topical indigo naturalis nanofibrous patch on psoriatic skin: A transdermal strategy for botanicals

Pengyu Wang [a,b], Junwei Gao [a], Shijie Guo [a], Hongmei Liu [c], Can Cao [a], Shihao Hong [a], Yu Sun [a], Chen Wang [a], Wei Xiao [d], Ping Song [b,***], Ning Li [a,**], Ruodan Xu [a,*]

[a] *Department of Biomedical Engineering and Technology, Institute of Basic Theory for Chinese Medicine, China Academy of Chinese Medical Sciences, Beijing, 100700, China*
[b] *Guang'anmen Hospital, China Academy of Chinese Medical Sciences, Beijing, 100053, China*
[c] *Key Laboratory of Medicinal Chemistry and Molecular Diagnosis of the Ministry of Education, College of Chemistry and Materials Science, Hebei University, Baoding, 071002, China*
[d] *National Key Laboratory on Technologies for Chinese Medicine Pharmaceutical Process Control and Intelligent Manufacture, Nanjing, 211100, China*

ARTICLE INFO

ABSTRACT

Indigo naturalis (IN) has been extensively used as a topical treatment for psoriasis. However, clinical applications of IN in ointment were hampered by its limited transdermal efficiency and dark stains. To address the aforementioned issues, nanopatches carrying IN were fabricated using poly(ε-caprolactone, PCL)/poly(ethylene oxide, PEO) and topically applied to psoriasiform skin. The ideal ratio of 5% PCL/PEO was established to be 80:20 (w/w), and 15% IN as payload was confirmed. Investigations on the three principal active components of IN release indicated that indirubin and tryptanthrin were released in bursts, while indigo was released in a limited and controlled manner. Further biological analyses confirmed a favorable biocompatibility of amphiphilic IN-PCL/PEO, which coincided with the intended therapeutic outcomes as measured by severity index scoring and pathological evaluations *in vivo*. The advantages of IN as nanopatches over ointment could be due to improved transdermal distribution of indirubin and tryptanthrin, resulting in effective management of epidermal hyperplasia and blood vessel remodeling. Meanwhile, due to the lower preservation of epidermal indigo, IN-PCL/PEO nanopatches caused no skin coloration. Similarly, during a 4-week topical treatment of IN-PCL/PEO nanopatches, the safety and anti-psoriatic benefits were obtained in an initial human test. The conversion of IN from topical cream to electrospun nanofibers opens up new avenues for bench-to-bedside translation of this herbal therapy and provides mechanistic insight into IN's roles in the management of psoriasis.

1. Introduction

Psoriasis vulgaris is a chronic immune-mediated inflammatory skin disorder, affecting approximately 90% of psoriasis patients [1,2]. Patients with psoriasis vulgaris frequently suffer from red and raised plaques covered by micaceous scales, which are always itchy and painful [3,4]. Typically, the scaly skin is histologically characterized by epidermal hyperplasia, blood vessel dilation, and leukocyte infiltration in the dermis [4]. Since the exact etiology of psoriasis remains unclear due to a complex interplay of genetic, immunologic, and environmental factors of this disease [1,4–6], the clinical management of psoriasis

vulgaris still leaves much to be desired. For instance, conventional systemic treatments using corticosteroids, cyclosporine, or methotrexate are known to have substantial side effects due to long-term applications [7–9]. Moreover, while biologic agents such as etanercept, infliximab, and ustekinumab are highly effective by targeting specific components of the immune response (TNF-a, IL17, IL12/23), their high cost, risk of infection linked to cancer incidence, and drug resistance have to be considered [4,10,11]. Alternatively, natural plant products have historically made a significant contribution to the pharmacotherapy of skin disorders; thus, the advancements of natural product-based therapies may contain crucial prospects to create new paths for psoriatic skin.

Indigo naturalis (IN) is an herbal medication derived from *Indigofera tinctoria* and other indigo plants' leaves and stems. IN is frequently used to treat a variety of inflammatory conditions, including psoriatic skin [12,13]. Indigo, indirubin and tryptanthrin, three primary components of IN, have previously been identified, contributing to a variety of pharmacological activities, such as immunological modulation, antioxidation, and antimicrobials [14–18]. However, the biological mechanism describing how the three chemicals react and exert their activities at target tissues remains largely unknown. Moreover, previous clinical studies have shown that IN can effectively relieve psoriasis symptoms by preventing the progression to severe conditions and promoting psoriatic skin recovery [19–23]; however, an extensive and repetitive oral administration of IN has been reported to be associated with mild liver dysfunction, abdominal pain and headache. To avoid such unfavorable side effects, IN ointments have been suggested and used as a topical medicine in recent years [19,24,25]. Though effective in treating psoriasis, the IN ointment as a semisolid oil is greasy and dark in color, leaving unpleasant residues on the skin and clothing. In addition to the unpredictable dosage of IN ointment, its practical utilization is frequently terminated due to poor patient compliance. Innovative IN dosage forms and increased transdermal bioavailability in the context of psoriasis are practically necessary to improve drug adherence.

Electrospun polymeric nanofibers have been demonstrated to be the most straightforward, easy and cost-effective drug-loading technique. Electrospinning has been utilized to create skin scaffolds and medicinal fibrous patches due to its high surface area, porosity, and ability to mimic the extracellular matrix [26–29]. The nanoscale dimension of electrospun fiber, in particular, allows fibers to make intimate contact with the stratum corneum (SC) of skin, promoting drug penetration into the epidermis [30]. Since the SC is composed of both hydrophilic "bricks" of keratin-filled corneocytes and hydrophobic "mortar" mixed with lamellar structurer of ceramides (50%), cholesterols (25%), fatty acids (15%) and low levels of phospholipids, amphiphilic nanofiber substrates have gained popularity in the fabrication of skin patches [31, 32]. Poly(ε-caprolactone) (PCL) is a widely used electrospun synthetic biodegradable polymer that allows for homogenous drug distribution in polymer matrix while also having desirable mechanical properties and long-term stability [33,34]. However, the hydrophobicity of PCL has limited its application in a largely hydrophilic bio-environment of drug delivery and necessitates hydrophilic modifications in general. Poly (ethylene oxide, PEO) is one of the well-known biocompatible, biodegradable and water-soluble polymers used in the pharmaceutical field to facilitate PCL solubilization. Despite extensive research into the feasibility of composite PCL/PEO nanofibrous scaffolds in tissue engineering and cancer therapy [35–38], few studies focused in detail on the dissolution and release of payloads incorporated into PCL/PEO in topical and transdermal drug delivery approaches.

In the preceding scenario, an optimal hybrid amphiphilic PCL/PEO nanofiber functionalized with IN (IN-PCL/PEO) was prepared. The appropriateness of a biocompatible fibrous nanopatch with excellent softness, bioadhesiveness and moisture retention for skin application was demonstrated. Three active components of IN were efficiently encapsulated into PCL/PEO nanofibers and then triggered to release by drops of water. IN-PCL/PEO topical treatments to imiquimod (IMQ)-induced psoriatic mice significantly reduced skin lesions and pathological psoriasis changes. The most significant therapeutic efficacy of IN-PCL/PEO nanopatches could be attributed to indirubin and tryptanthrin transdermal delivery, which are involved in the control of epidermal hyperplasia and blood vessel remodeling, two features that distinguish the effectiveness of IN-PCL/PEO from IN ointment in psoriatic skin. It is worth noting that IN-PCL/PEO nanopatches successfully solved the problem of skin coloration by lowering epidermal indigo absorption. The substantial results of electrospinning-based IN nano-encapsulation deliver additional benefits such as improved IN bioavailability and storage convenience, reduced medication time and cost, and increased patient compliance. The conversion of IN from topical cream to electrospun nanofibers opens up new avenues for bench-to-bedside translation of this herbal medicine and provides an insightful understanding of the mechanisms of IN in the management of psoriasis.

2. Materials and methods

2.1. Materials

Indigo naturalis (IN) was purchased from Juyaotang Pharmaceutical Co., Ltd. (Z2111002, Anguo, China). The reference standard of indigo (98% purity), indirubin (≥97% purity) and tryptanthrin (≥98% purity) were purchased from Yuanye Bio-Technology (Shanghai, China). PCL of 80 kDa (in number Mn) PEO (Mv = 300 kDa) and sodium dodecyl sulfate (SDS) were obtained from Sigma-Aldrich (St. Louis, MO, USA). 1,1,1,3,3,3-Hexafluoro-2-propanol (HFIP), *N, N*-dimethylformamide (DMF), dimethyl sulfoxide (DMSO) and ethyl acetate were supplied from Aladdin Biochemical Technology (Shanghai, China). Methanol and acetonitrile (HPLC grade) were purchased from Thermo Fisher Scientific (Fair Lawn, NJ, USA).

2.2. Electrospinning

PCL and PEO were dissolved in HFIP at various ratios listed in Table S1 and stirred overnight to obtain a homogeneous solution. IN (5%, 10%, 15%, 20%, 25%, 30%, and 50% w/w) was added slowly into the PCL/PEO while mixing. Solutions were transferred to a 5 mL syringe and mounted on the syringe pump in an electrospinning machine (ET-2535DC, Ucalery, Beijing, China). A positive high voltage was connected via an alligator clip to a needle, while the collecting plate was covered with an aluminum fold and connected to a ground. Process parameters were fixed at a voltage of 7 kV, flow rate of 0.15 mm/min, and distance from needle tip to collector of 12 cm. The temperature was 32 °C and the humidity 20–30%. The fabricated nanofibrous membranes were frozen overnight and then freeze-dried using a freeze-drying system (LGJ-10C, Foring Technology, Beijing, China).

2.3. Scanning electron microscopy (SEM)

The nanofibrous membranes and HaCat cells on electrospun mats were sputter coated with a thin layer of gold before examination. The microstructures of the samples were observed by using a field emission scanning electron microscopy (Phenom Pharos G2, Eindhoven, Netherlands) at an accelerating voltage of 10 kV. The diameters of resulting fibers were measured at random locations on each fiber and the average diameter was calculated using image analysis software (Image J, NIH, USA).

2.4. Fourier transform infrared spectroscopy (FTIR)

The chemical bonds of IN, indigo, indirubin, tryptanthrin, PCL/PEO, IN-PCL/PEO, indigo-PCL/PEO, indirubin-PCL/PEO and tryptanthrin-PCL/PEO nanofibers were investigated using the Spectrum Two FTIR spectrometer (Perkin-Elmer, Waltham, Mass, USA). The infrared spectra were recorded at (4000–400) cm^{-1} region with a resolution of 4 cm^{-1}.

2.5. Water contact angle

The wettability of the membrane was measured using a contact angle instrument (Theta Flow, Biolin Scientific, Espoo, Finland) by dropping 3 μL of ddH$_2$O onto the fiber membrane. The measurement was performed three times and the average value was calculated.

2.6. High-performance liquid chromatography (HPLC)

The contents of indigo, indirubin and tryptanthrin in the samples

were determined by HPLC (Agilent Technologies, Palo Alto, CA, USA), respectively. In chromatography, C18 column was used as the stationary phase (Agilent, Stable Bond 300, 250 mm × 4.6 mm, 5 μm), and the mobile phase was either composed of acetonitrile and ddH$_2$O (53:47, v/v), or methanol and ddH$_2$O (60:40, v/v) at a flow rate of 1 mL/min with the retention time being 5.4 min, 6 min and 4.5 min, respectively. The amounts of indigo, indirubin, and tryptanthrin were quantified at 288 nm, 288 nm and 254 nm, respectively.

2.7. In vitro drug release

A release study was made to determine indigo, indirubin and tryptanthrin release profile from IN-PCL/PEO in a 5 mL solution with 50% ethanol (pH 5.5) containing 2% (w/v) SDS at 34 °C. 1 mL solution from each sample was collected at 5, 10, 15, 20, 25, 30 min and 1, 2, 3, 6, 12 h for a period of 24 h, meanwhile 1 mL fresh solution was added to each sample to maintain a constant volume of 5 mL. The amount of released indigo, indirubin and tryptanthrin was analyzed by HPLC.

2.8. Skin permeation and retention studies

The *ex vivo* skin permeation and retention of indigo, indirubin and tryptanthrin from IN-nanofiber or IN ointment were investigated using Franz-type glass diffusion cells (Huke, Jiangsu, China) with an effective diffusion area of 3.14 cm^2. The excised psoriatic mouse skin was equilibrated in saline for 30 min after removing subcutaneous fat and mounted between the donor and receptor compartments with the stratum corneum facing upward into the donor. IN ointment (in vaseline) or IN-PCL/PEO was placed onto the skin in the donor chamber, sealed with Parafilm® (Bemis NA, Neenah, USA). A clean, dried receptor cell was filled with 50% ethanol buffer (pH 5.5) containing 2% SDS and stirred at 200 rpm to equilibrate at 34 °C. 30 min later, samples were harvested from the receptor cells for HPLC tests. The skin samples were collected for drug retention assays, in which the epidermis was separated from the dermis using 0.25% Trypsin-EDTA (Gibco, Grand Island, NY, USA) and tissue samples were ground using a cryogenic grinder (JXFSTPRP-II, Jingxin Industrial Development Co., Ltd., Shanghai, China). IN components retained in the skin were extracted with ethyl acetate three times and the organic layers were concentrated under vacuum. The precipitation was dissolved in 200 μL DMSO for HPLC analysis.

2.9. Cell culture

Human keratinocytes (HaCat) were obtained from FuHeng Cell Center (Shanghai, China) and grown in RPMI-1640 medium (Gibco) supplemented with 10% fetal bovine serum (FBS, Gibco) and 1% penicillin/streptomycin (P/S, Gibco). Human umbilical vein endothelial cells (HUVEC) were purchased from BeNa Culture Collection (BNCC, Beijing, China) and expanded in complete endothelial cell medium (ECM, ScienCell, San Diego, CA, USA) supplemented with 10% FBS (ScienCell), 1% ECGS (ScienCell) and 1% P/S (ScienCell). All cells were incubated at 37 °C in a humidified atmosphere of 5% CO$_2$. Cells were enzymatically treated with Trypsin-EDTA (0.25%, Gibco) for passaging every 5–7 days.

2.10. Cell viability and proliferation

Live/dead staining was performed to visualize the number of viable and non-viable HaCat cells on the fiber membranes. After 24 h cultivation on the nanofibrous membranes, samples were stained with PBS containing 2 μM Calcein-AM (Invitrogen, Carlsbad, CA, USA) and 4 μM propidium iodide (PI, Sigma) for 20 min at 37 °C. Calcein-AM reacts with intracellular esterase of live cells to emit green fluorescence, while PI interacts with DNA of dead cells with red fluorescence. Digital images of viable (green) and dead (red) cells were visualized using an Olympus FV3000 confocal laser microscope (Tokyo, Japan).

Cell proliferation was assayed with CellTiter96®Aqueous One Solution Cell Proliferation Assay Kit (Promega, Madison, WI, USA). Briefly, cells were seeded and cultured with growth medium supplemented with EGF (0–400 ng/mL) (Abcam, Cambridge, MA, USA) or various compounds (indigo, indirubin and tryptanthrin) as indicated concentrations at a density of 1.5×10^4 HaCat cells/cm^2 or 1.8×10^4 HUVEC cells/cm^2 for 48 h. Then, cell culture medium was removed, MTS-reagent was added in each well and incubated for 3 h. The same volumes of culture medium and MTS-reagent without cells were also incubated as the background. 100 μL of the solution was transferred into a 96-well plate, and the absorbance at 490 nm was measured for each well. Alternatively, HaCat were seeded at a density of 5×10^4 cells/cm^2 on different fiber membranes (PCL/PEO, 5% IN-PCL/PEO, 10% IN-PCL/PEO, 15% IN-PCL/PEO and 20% IN-PCL/PEO) with growth medium. The cell proliferation was examined on day 1, 3, 5 after incubation.

2.11. Immunocytochemistry

The morphology of cells cultured on nanofibers was characterized by confocal fluorescence microscopy. Each sample was fixed with paraformaldehyde (Solarbio, Beijing, China) and rinsed with PBS. Triton X-100 (Sigma) was added into the samples and further blocked with 1% bovine serum albumin (Sigma) in PBS. The F-actin and nuclei of cells were immune-stained with Alexa Fluor 488 Phalloidin (Thermo Fisher Scientific) and DAPI (Sigma), respectively. The cells and cell-laden constructs were visualized using a confocal laser microscope (Olympus FV3000).

2.12. Cell cycle arrest analysis by flow cytometry

PI staining was performed to evaluate the induction of cell cycle arrest in keratinocytes of HaCat and then analyzed by flow cytometry [39]. HaCat cells (2×10^5 cells/well) were seeded in 6-well plate and treated with EGF (10 ng/mL), and then incubated with indigo (30 μM), or indirubin (30 μM), or tryptanthrin (100 μM) for 24 h. After trypsinization, the cells were fixed in 70% ethanol and stored at −20 °C. Later, the ethanol-fixed cells were washed with PBS and incubated in a staining buffer which contains PI and RNase enzyme. The cells were then measured using the BD Accuri C6 flow cytometer (BD biosciences, CA, USA) and analyzed by FlowJo software (V.10.4, BD).

2.13. Apoptosis assay

To detect cell apoptosis, the assay was performed following the manufacturer's protocol using the Alexa Fluor 488 Annexin V/Dead cell apoptosis kit (Thermo Fisher Scientific). Briefly, HaCat cells were seeded at a density of 2×10^5 cells/well in 6-well plate. The cells were stimulated with EGF (10 ng/mL) and treated with indigo, indirubin, or tryptanthrin for 24 h. Afterwards, the cells were washed with cold PBS and resuspended in 1X binding buffer. Then, Annexin V and PI were added and incubated with cells for 15 min in the dark at room temperature (RT). Finally, the cells were evaluated using the BD Accuri C6 flow cytometer, and FlowJo was used to analyze the percentage of cells in four populations, including FITC$^-$/PI$^-$ (living cells), FITC$^+$/PI$^-$ (early apoptotic cells), FITC$^+$/PI$^+$ (late apoptotic cells), and FITC$^-$/PI$^+$ (necrotic cells).

2.14. Tube formation assay

The extracellular matrix (ECM) gel based capillary tube formation assay was used as *in vitro* measurement of angiogenesis. This was performed following the manufacturer's instructions, using precooled tubes and tips to prevent premature gelling. Briefly, 10 μL Matrigel (R&D Systems, MN, USA) was placed in each well of angiogenesis μ-slides (Ibidi GmbH, Gräfelfing, Germany) for 1 h at 37 °C. Then, HUVECs at a density of 6×10^3 cells/well were added. 2 h later, the basal medium

was replaced by the medium containing 0–70 ng/mL recombinant human FGF-basic (bFGF, R&D) for 4–7 h. For disruption assay, various concentrations of indigo, indirubin or tryptanthrin as indicated, or 15 μM sulforaphane (Sigma) were added into the wells along with 50 ng/mL bFGF and incubated for 6 h at 37 °C in a humidified atmosphere with 5% CO_2. Cells were stained with Alexa Fluor 488 Phalloidin and DAPI, and the formation of capillary tubes was photographed using Zeiss Axio Observer microscope (Göttingen, Germany) and analyzed with the software AngioTool (v 0.6a (64 bits)) [40].

2.15. Animal model and treatment

BALB/c mice (male, 6–8 weeks, 20 ± 2 g) were purchased from Beijing Vital River Laboratory Animal Technology CO., Ltd. (Beijing, China). All experimental animals were group-housed with free access to food and water in a controlled environment with constant temperature and a standard light/dark cycle throughout the experimental period. All animal studies were conducted according to the National Guidelines for Care of Laboratory animals and performed in accordance with institutional regulations with approval of experimental protocols by the Institutional Animal Care and Use Committee of the Institute of Basic Theory for Chinese Medicine, China Academy of Chinese Medical Sciences.

Imiquimod (IMQ) is a TLR7/8 ligand and a potent immune activator, topical application of IMQ could develop the psoriasis-like mouse model. The mice were divided into 8 groups, which were all treated with IMQ (62.5 mg of 5% IMQ cream Aldara®, 3 M Pharmaceuticals, St. Paul, MN) on the shaved back every 24 h for 7 days. In addition to the control group (without IMQ treatment) and model group (IMQ treatment only), the inflamed skin area of other 6 groups were also treated once daily with clobetasol propionate (CP), IN ointment, PCL/PEO, 5% IN-PCL/PEO, 10% IN-PCL/PEO, 15% IN-PCL/PEO and 20% IN-PCL/PEO, respectively. The 3 cm × 2 cm fibers were topically applied with drops of water on the skin for 30 min. The body weight and images of skin lesions were recorded every day. On the 8th day, mice were sacrificed and the skin samples from the back were harvested for the pathological experiments.

2.16. Evaluation of the severity of psoriatic skin lesion

Based on the clinical psoriasis area and severity index (PASI), an objective scoring system was used to evaluate the severity of inflammation on the mice dorsal skins. Erythema and scaling scores were obtained daily by blindly scoring with a scale from 0 to 4 (0-none; 1-slight; 2-moderate; 3-marked; 4-very marked). The scores for the scales and erythema were added to obtain the total score ranging from 0 to 8. The score was taken once a day for 7 days from the date of administration. In addition, the thickness of lesional skin was monitored by optical coherence tomography (OCT, Moting, Guangdong, China) throughout the whole experimental period (day 0, 1, 3, 5, 7). Three mice in each group were randomly selected and the epidermal thickness at the lesion was dynamically observed and measured by ImageJ.

2.17. Hematoxylin and eosin (H&E) staining

At the end of the experiment, skin, liver, kidney and spleen from mice were fixed with 4% paraformaldehyde for 48 h, embedded in paraffin, and then sectioned into 4-μm slices using a microtome (Leica, Nussloch, Germany). After deparaffinized and rehydrated, the tissue sections were stained with hematoxylin-eosin staining solution (Solarbio), according to manufacturer's protocol. All images were taken using the ScanScope slide scanner (Aperio, CA, USA) with an image analysis system (Aperio V.10.2).

2.18. Immunohistochemistry (IHC)

For IHC staining, the hydrated sections were treated with citrate antigen retrieval solution (Beyotime, Shanghai, China) at 95 °C for 15min and cooled down at RT. 5% goat serum in PBS was used to block the nonspecific binding sites after inactivating endogenous peroxidase. Primary antibodies of anti-Ki67 (ab16667, 1:400), or anti-CD68 (ab125212, 1:2000), or anti-CD31 (ab124432, 1:1000) from Abcam were used for overnight staining at 4 °C. Next, sections were incubated with secondary antibody of goat anti-rabbit IgG (Zhongshan Golgen Bridge Biotechnology, Beijing, China) for 30 min at RT. Finally, the sections were stained with fresh diaminobenzidine (Zhongshan Golgen Bridge Biotechnology) and counterstained with hematoxylin. All images were taken using the ScanScope slide scanner with Aperio ImageScope analysis software.

2.19. Preliminary in vivo test of topical application

An initial *in vivo* test was conducted on three patients with mild-to-moderate plaque psoriasis to evaluate the safety and efficacy of IN-PCL/PEO nanopatches. The study design was approved by the Institutional Ethics and Research Committee of the Institute of Basic Theory for Chinese Medicine, China Academy of Chinese Medical Sciences (Approval No. 2022-KY-EC-002). Inclusion criteria are defined as patients with mild-to-moderate plaque psoriasis aged between 18 and 65 years, and exclusion criteria are set to be patients with guttate, severe psoriasis or other inflammatory skin diseases, or patients who received any topical or systemic treatment for psoriasis one month before the start of the study, or pregnant or lactating females. As a preliminary test, one female and two males were enrolled according to inclusion criteria and exclusion criteria. After signing the informed consent form, all data including age, gender, occupation, residence, marital status, family history of psoriasis, age at onset, duration of disease, precipitating and exacerbating factors and previous treatment for psoriasis were recorded and documented. The lesioned region was randomly selected from the body. For each treatment, 30 mg IN-PCL/PEO nanopatch covering over a surface area of 9 cm^2 was applied topically with drops of water for 30 min, twice *per* day for up to 4 consecutive weeks. Safety including itching and burning sensation was assessed, and tolerability was evaluated based on subject reports of discomfort during the treatment. The severity of plaque appearance was determined by dermatologists using the PASI score by grading the severity of erythema, infiltration and scaling under the 0-to-4 scale, which was compared to corresponding baseline values obtained at the first visit.

2.20. Statistical analysis

Data are represented as mean value ± the standard error of the mean (SEM) and were analyzed with the one-way analysis of variance (ANOVA) with the Bonferroni post hoc test. Values are considered to be significant at $p < 0.05$. All statistical analysis was performed, and figures were created using Prism 9 (GraphPad, San Diego, CA, USA).

3. Results and discussion

3.1. Preparation and physical characterizations of IN-PCL/PEO nanopatch

To increase the bioavailability of IN for topical psoriasis treatment, PCL/PEO copolymers were fabricated as transdermal drug delivery systems by blending electrospinning. Following the determination of the optimal 5% PCL/PEO composition of 80:20 (w/w) (Fig. S1 and Table S1), the proper incorporation of various concentrations of IN (5%, 10%, 15%, 20%, 25%, 30%, 50%) was investigated by taking into account the achievement of morphologically smooth, bead-free and randomly oriented nanofibers (Fig. 1A–D and Fig. S2). By SEM, the
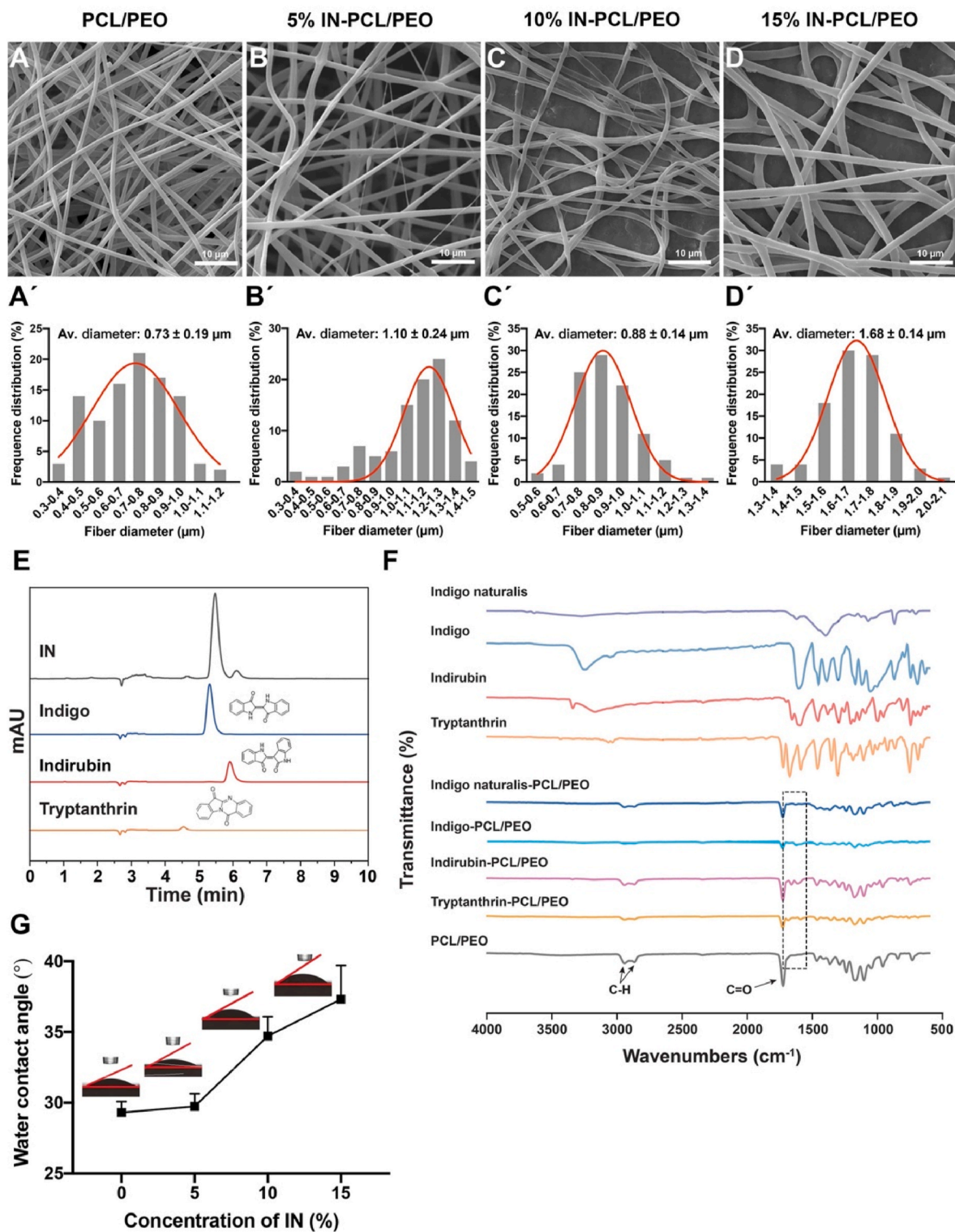
Fig. 1. Characterizations of electrospun nanopatches. (A–D) SEM images of PCL/PEO (A), 5% IN-PCL/PEO (B), 10% IN-PCL/PEO (C), and 15% IN-PCL/PEO (D) with corresponding diameter distributions of PCL/PEO (A′), 5% IN-PCL/PEO (B′), 10% IN-PCL/PEO (C′), and 15% IN-PCL/PEO (D′). Scale bar: 10 μm. (E) HPLC analysis of IN, with its major compounds indigo, indirubin and tryptanthrin as reference standards. (F) FTIR spectra of IN, indigo, indirubin, tryptanthrin, electrospun PCL/PEO, and the PCL/PEO blended with IN, or indigo, or indirubin or tryptanthrin. (G) Water contact angle measurements of PCL/PEO nanofibers loaded with 5%, 10% or 15% IN. Bars represent mean ± SEM of 3 independent assays.

smooth and bead-free fiber structure was achieved only when IN was less than 15% (Fig. 1A–D). When the loaded IN (20–50%, Fig. S2) increased above 15%, more and bigger clumps of IN were formed due to a relatively low solubility of IN in electrospinning solution. Compared to

the average diameter of PCL/PEO vehicle fibrous membrane, which was acquired to be 0.73 ± 0.19 μm (PCL/PEO, Fig. 1A and A′), subsequent incorporations of IN from 5% to 15% slightly enhanced the size of fiber, showing 1.10 ± 0.24 μm for 5% IN-PCL/PEO (Fig. 1B and B′), 0.88 ±

0.14 μm in 10% IN-PCL/PEO (Fig. 1C and C'), and 1.68 ± 0.14 μm for 15% IN-PCL/PEO (Fig. 1D and D'). To validate that IN had been successfully loaded into the PCL/PEO nanofibrous membrane, the three principal active constitutes of IN, indigo, indirubin and tryptanthrin, were evaluated by both HPLC (Fig. 1E) and FTIR (Fig. 1F). In accordance with previous studies [41], IN could be easily identified using HPLC by comparing it to reference standards (Fig. 1E). Further quantitative analysis revealed that IN was composed of 2.22 ± 0.46% indigo, 0.33 ± 0.02% indirubin and 0.03 ± 0.01% tryptanthrin. In complement to HPLC, FTIR that provides information on molecular structure and chemical environments was carried out. In agreement with previous reports on PCL and PEO [42], typical FTIR spectra of PCL/PEO could be recorded, displaying both symmetric and asymmetric stretching peaks of $-CH_2-$ located at 2945 cm^{-1} and 2858 cm^{-1}, and symmetric stretching vibration peak of C=O at 1726 cm^{-1}. The C=O group peak at 1726 cm^{-1} was seen solely in PCL, whereas symmetric stretching vibration of C–O–C produced the PEO characteristic peak at 1103 cm^{-1} (Fig. 1F). For

IN, a large absorption band in the range of 1400–1620 cm^{-1} was observed, which might be explained by the stretching vibration of the benzene ring of aromatic components. However, no distinct characteristic peaks were observed for IN incorporated into PCL/PEO, which was mostly likely due to a relatively low content of active components in fibers. To address this further, we attempted to integrate indigo, indirubin and tryptanthrin into PCL/PEO separately and then examined their FTIR spectrum. As shown in the lower panels of Fig. 1F, the 1586-1701 cm^{-1} spectral range, which is assigned to the stretching vibration of the conjugated system of C=C, C=O, and N–H groups, was responsive to all three tested IN molecules, exhibiting subtle bands at 1682 cm^{-1}, 1628 cm^{-1}, 1589 cm^{-1} in indigo-, indirubin-, or tryptanthrin-loaded PCL/PEO fibers respectively, supporting a success encapsulation of IN into PCL/PEO. Altogether, this set of data confirmed the miscibility of IN or its key components with PCL/PEO as electrospinning nanofibers.
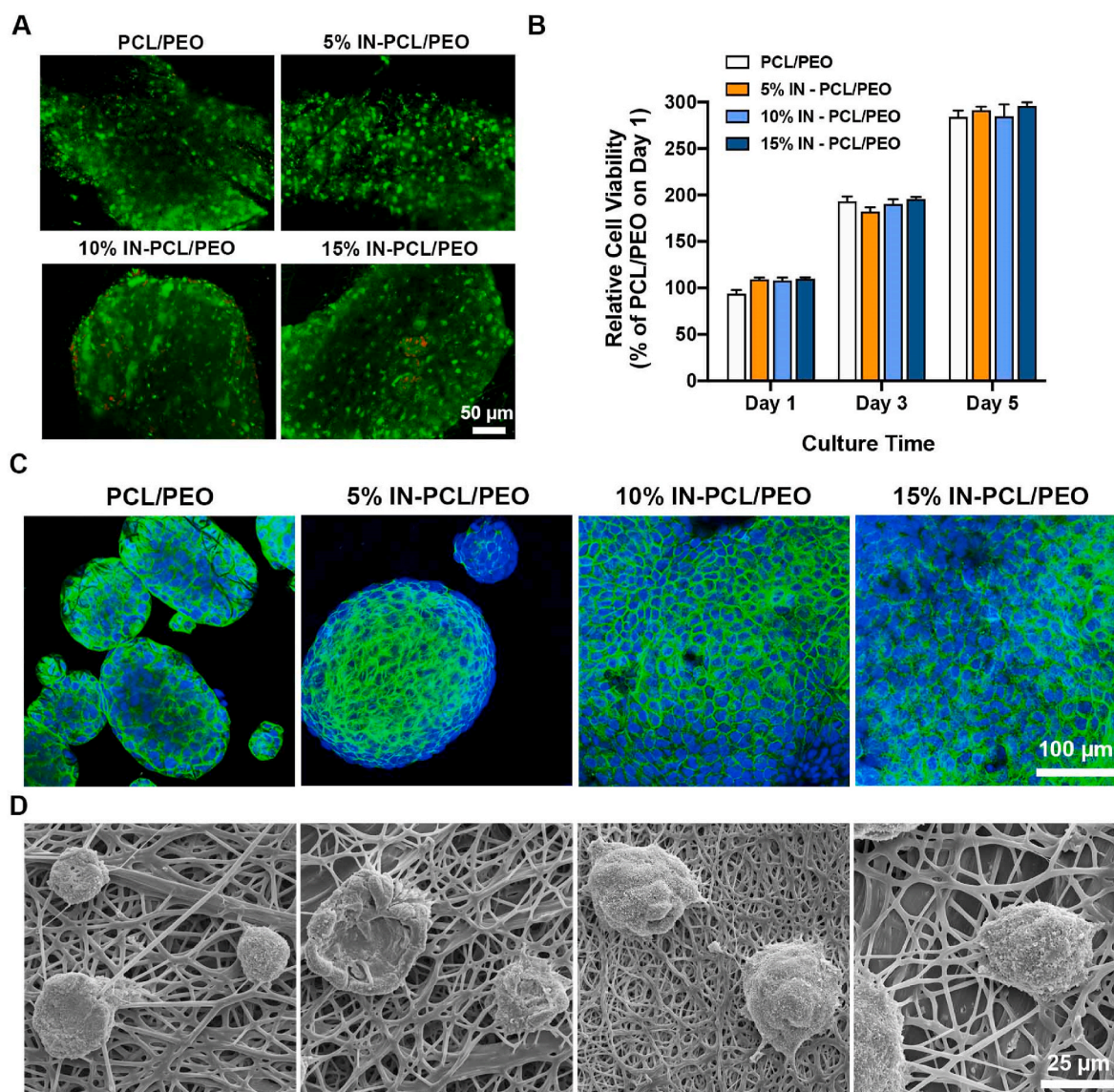

Fig. 2. Biocompatibility of electrospun nanopatches. (A) Micrographs for live (green)/dead (red) cell assays 1 day after seeding HaCat onto electrospun PCL/PEO, 5% IN-PCL/PEO, 10% IN-PCL/PEO, or 15% IN-PCL/PEO. Scale bar: 50 μm. (B) HaCat cell viability after incubating with PCL/PEO, 5% IN-PCL/PEO, 10% IN-PCL/PEO, or 15% IN-PCL/PEO for 1, 3 and 5 days. (C) Fluorescence staining of cytoskeletons (green) of HaCat cells after 3 days of culture on PCL/PEO, 5% IN-PCL/PEO, 10% IN-PCL/PEO, or 15% IN-PCL/PEO, with nuclei counterstained in blue. Scale bar: 100 μm. (D) Representative SEM images presenting HaCat cells on the surface of the electrospun membrane of PCL/PEO, 5% IN-PCL/PEO, 10% IN-PCL/PEO, or 15% IN-PCL/PEO after 5 days of cell culture. Scale bar: 25 μm. (For interpretation of the references to colour in this figure legend, the reader is referred to the Web version of this article.)

3.2. Surface hydrophilicity of IN-PCL/PEO nanopatch

The electrospun IN-PCL/PEO nanopatch is constructed as "dry membrane" which requiring hydration prior to drug release and permeation over the skin barrier. Hence, we determined the surface wettability and hydrophilicity of nanopatches *via* measuring contact angle between the water droplets and membrane surface, with a low contact angle indicating high hydrophilicity of the tested membrane. Because PEO is known to absorb water, its blending with PCL made the surface of membranes to be more hydrophilic. This was demonstrated in the non-drug-loaded PCL/PEO composition of 80:20 (w/w) in Fig. 1G. Meanwhile, as IN contains nonpolar side groups, with the amount of IN loaded into PCL/PEO membrane increased, the water contact angle was found to grow, resulting in a gradually enhanced hydrophobic behavior of IN nanopatches. Therefore, the addition of PEO improved PCL wettability, which could be further modified by IN contents, and this amphiphilic behavior of IN-PCL/PEO was truly a desired feature for topical drug delivery.

3.3. In vitro biocompatibility of IN-PCL/PEO nanopatches

The IN-PCL/PEO was then tested for *in vitro* biocompatibility using the human keratinocyte (HaCat) line as a skin cell model. Live/dead cells assays provide direct information on IN-PCL/PEO cytotoxicity. By staining live cells with calcein-AM (green), and dead cells with PI (red), a 24-h incubation of HaCat with IN-loaded PCL/PEO did not significantly impact cell viability (Fig. 2A). This was additionally supported by quantitative MTT assays, which depict the metabolic activity of cells (Fig. 2B). A similar pattern of HaCat growth in PCL/PEO and IN-PCL/PEO was achieved by extending the incubation periods from 1 day to 5 days, indicating that IN-PCL/PEO has a favorable biocompatibility. More in-depth investigations were carried out by directly visualizing cell adhesion and spreading on nanofibers. As shown in Fig. 2C, after a 3-day exposure to nanopatches, green fluorescence of FITC-phalloidin signifying cell structure and integrity revealed a well-organized network of HaCat cytoskeleton. Moreover, after 5 days of incubation, single cell morphology and the cell-fiber interaction at the nanoscale captured by SEM manifested that HaCat on nanofibers became more spherical, and a physical contact among cells was established due to the formation of cellular pseudopodia (Fig. 2D), verifying that IN-PCL/PEO nanopatches are highly biocompatible.

3.4. In vitro drug release of IN-PCL/PEO nanopatch

To better understand the therapeutic potential of IN, we first assessed the dynamic release performance of indigo, indirubin and tryptanthrin. As evidenced in Fig. 3A–C, approximately 8.5% of indigo was released from PCL/PEO nanofibers during the first 30 min followed by a gradual liberation of indigo to 11.1% at 24 h. In comparison, a considerably faster profile of 46.9% indirubin and 66.4% tryptanthrin release was recorded within the first 30 min, which steadily increased to 63.0% indirubin and 73.4% tryptanthrin release at the end of 24 h. The result of drug release demonstrated a highly efficient liberation of indirubin and tryptanthrin compared to indigo. In addition, the more efficient and prominent initial burst release of IN components relative to that of 24 h implied that a 30-min application of nanopatches could be sufficient to meet therapeutic demands.

3.5. Amelioration of psoriatic phenotypes by IN-PCL/PEO nanopatch in IMQ-induced mice

To test the anti-psoriatic capability of IN-PCL/PEO nanopatches *in vivo*, PCL/PEO loaded with 5%, 10%, or 15% IN was applied topically for 30 min per day to the shaved back skin of BALB/c mice subjected to IMQ cream for 7 consecutive days (Fig. 4A). Meanwhile, as positive and comparison controls, CP and IN ointment were used, respectively. Throughout the experimental period, mice were weighed daily, and on the day of assessment, mice in IMQ model group had a significant loss of body weight (Fig. 4B). Weight loss caused by IMQ could be entirely reversed by 15% IN-PCL/PEO (Fig. 4B), which was in agreement with the recovery of psoriasis-like skin lesions of experimental mice (Fig. 4C and Fig. S3). Notably, when compared to IMQ-induced animals that did not receive any pharmacological therapy, psoriatic skin treated with CP, IN ointment, PCL/PEO, or IN-PCL/PEO demonstrated an overall reduction in both skin scales and erythema, albeit to a varied degrees at day 7. Typically, topical applications of IN ointment only resulted in a slight restoration of erythema and scaling compared to IMQ model mice, but the psoriatic skin lesion was strikingly stained dark blue by IN. Moreover, despite the fact that the PCL/PEO carrier greatly ameliorated psoriasis-like symptoms, the IMQ-induced skin damages were less severe in IN-PCL/PEO-treated mice. The interpretation of the macroscopic appearance of skin lesions was validated with the grade of severity assessed by PASI score, which incorporates the evaluation of erythema and scaling (Fig. 4E, F and G).

To further demonstrate the dosage-effect of IN in IMQ mice model, we additionally compared 15% and 20% IN-PCL/PEO nanopatches in terms of the improvement of psoriasis-associated changes (Fig. S4). Prior to *in vivo* study, a similar pattern of HaCat growth between 15% and 20% IN-PCL/PEO was observed during 5 days of incubation, indicating a biocompatibility of 20% IN-PCL/PEO (Fig. S4A). Similarly, 20% IN-PCL/PEO could also reverse mice weight loss caused by IMQ (Fig. S4B). According to macroscopic observation of skin lesions (Fig. S4C), PASI (Figs. S4D–F) and H&E histology (Fig. S4G), both 15% and 20% IN-PCL/PEO nanopatches are therapeutically effective, with no
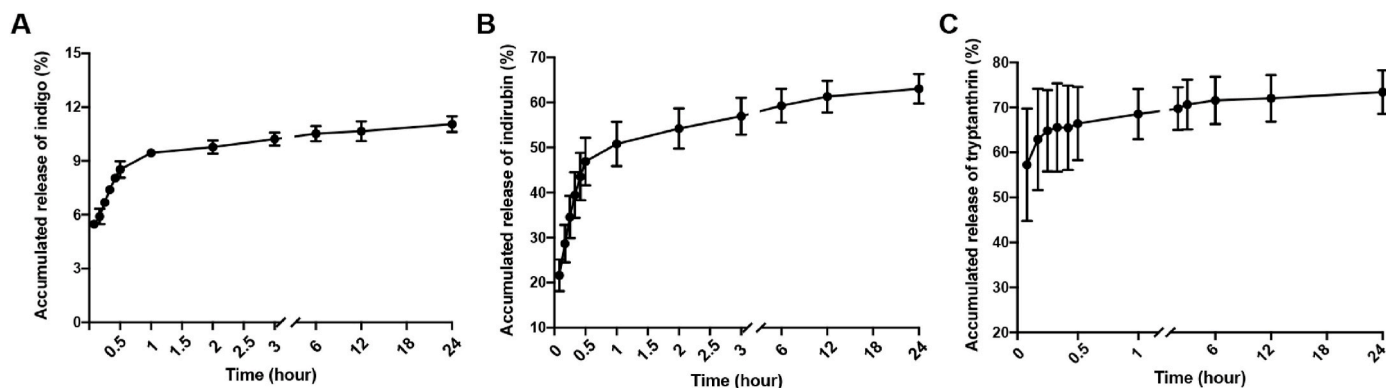

Fig. 3. Release profile of indigo, indirubin and tryptanthrin from IN-PCL/PEO nanopatches. Cumulative drug release curves of indigo (A), indirubin (B) and tryptanthrin (C) from IN-PCL/PEO nanofibers. The drug release study was performed in 50% ethanol (pH 5.5) containing 2% (w/v) SDS, and the amount of released drugs was estimated by HPLC analysis. Bars represent mean ± SEM of 3 independent assays.
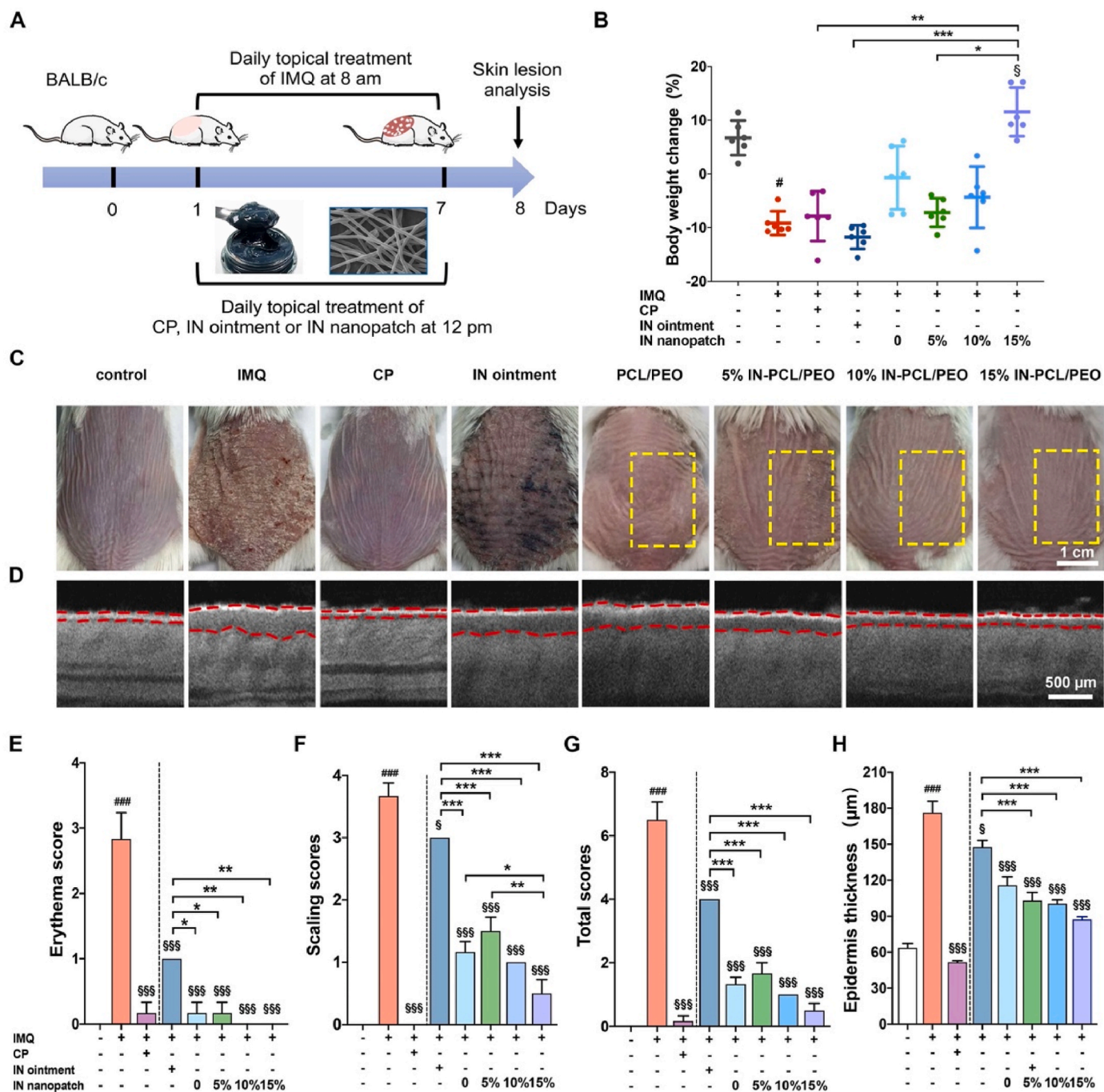
Fig. 4. Amelioration of psoriatic phenotypes by IN-PCL/PEO nanopatches in IMQ-induced mice. (A) Experimental design to evaluate the anti-psoriasis efficacy of IN-PCL/PEO nanopatches in IMQ-induced psoriasis-like mice. (B) Changes of body weight of experimental mice at the end of experimental periods (n = 6). (C) The macroscopic appearance of dorsal shaved skin of mice treated with indicated formulations. Dotted boxed in yellow represent the location where the nanopatch was attached. Scale bar: 1 cm. (D) OCT images of the skin areas of mice treated with indicated formulations *in vivo*. Dashed red lines in images indicate the skin epidermal thickness. Scale bar: 500 μm. (E–G) Evaluations of erythema (E), scaling (F) and total PASI (G) of IMQ-induced psoriatic dorsal skin in mice treated with indicated formulations (n = 6). (H) Epidermal thickness was quantified according to OCT images (n = 3). Data are presented as the mean ± SEM. $^{###}p < 0.005$ compared with control without any drug treatment; $^{§}p < 0.05$ and $^{§§§}p < 0.005$ compared with IMQ; $^{*}p < 0.05$, $^{**}p < 0.01$, and $^{***}p < 0.005$ between treatments as indicated. (For interpretation of the references to colour in this figure legend, the reader is referred to the Web version of this article.)

statistical difference between the two groups. This set of results suggests that 15% IN is the optimal dosage for electrospinning and 15% IN-PCL/PEO maybe the most cost-effective use for treating IMQ-induced psoriasis like dermatitis.

Considering that the skin epidermal thickness could not be directly determined by symptoms, we supplemented with OCT, a non-invasive *in vivo* technique that provides cross-sectional evaluations of the skin

structure (Fig. 4D and H and Fig. S5). In accordance with PASI evaluations, IN-PCL/PEO alleviated epidermal hyperplasia in a dose-dependent manner ($-34.3 \pm 20.4\%$ in PCL/PEO, $-41.6 \pm 19.2\%$ in 5% IN-PCL/PEO, $-43.1 \pm 8.9\%$ in 10% PCL/PEO, and $-50.5 \pm 6.6\%$ in 15% IN-PCL/PEO), and the reduction of epidermal thickness by IN ointment ($-16.2 \pm 15.7\%$) was apparently less satisfactory compared to nanopatches. Taken together, we affirmed that 30 min per day IN-PCL/

PEO nanopatch treatment was more effective and superior to IN cream in mitigating psoriatic phenotypes without any signs of lesion coloration.

3.6. Inhibition of psoriatic hyperplasia and inflammation by IN-PCL/PEO nanopatch in IMQ-induced mice

To have a deeper insight into therapeutic efficacies of IN-PCL/PEO on psoriatic alterations, pathological examinations were accordingly performed and quantified (Fig. 5A and B). Firstly, for psoriatic hyperplasia, the H&E staining could match the pattern of epidermal thickness acquired by OCT (Fig. 4D), showing a nearly 3-fold hyperplasia in IMQ-exposed skin that was substantially suppressed by IN-PCL/PEO nanopatches. Since epidermal thickening is associated with high cell proliferation in the basal layer and irregular keratinocyte maturation, we therefore quantified cell proliferation by Ki67, a nuclear protein expressed in proliferating cells. Consistent with epidermis thickness, IN-PCL/PEO nanopatches significantly reduced the amount of Ki67

immunoreactive cells, a phenomenon comparable to the CP positive control. In comparison with IN ointment, IN-PCL/PEO nanopatches of different dosages protected more efficiently against hyperproliferation in psoriatic skin. Secondly, along with keratinocyte proliferation, angiogenesis is deeply involved in the pathogenesis of psoriasis [43–45]. As pathologically revealed, the lesional skin of mice exhibited dramatically dilated blood vessels with a significantly intense staining of CD31-positive endothelial cells in response to IMQ. The provision of IN, in the form of both cream and nanopatches, could reduce IMQ-induced angiogenesis to approximately half, among which nanopatches containing 10% and 15% IN achieved the most successful anti-angiogenic results, highlighting the significance of IN-PCL/PEO nanopatches in the prevention of hyperproliferation. Thirdly, in the respect of inflammation of psoriatic tissues, macrophages are the predominant inflammatory cells participating in this process. By detecting CD68, a high degree of resident dermal macrophages was observed following IMQ exposure compared to normal skin, whereas topical treatment with IN restrained inflammatory infiltrates in all relevant groups without a clear
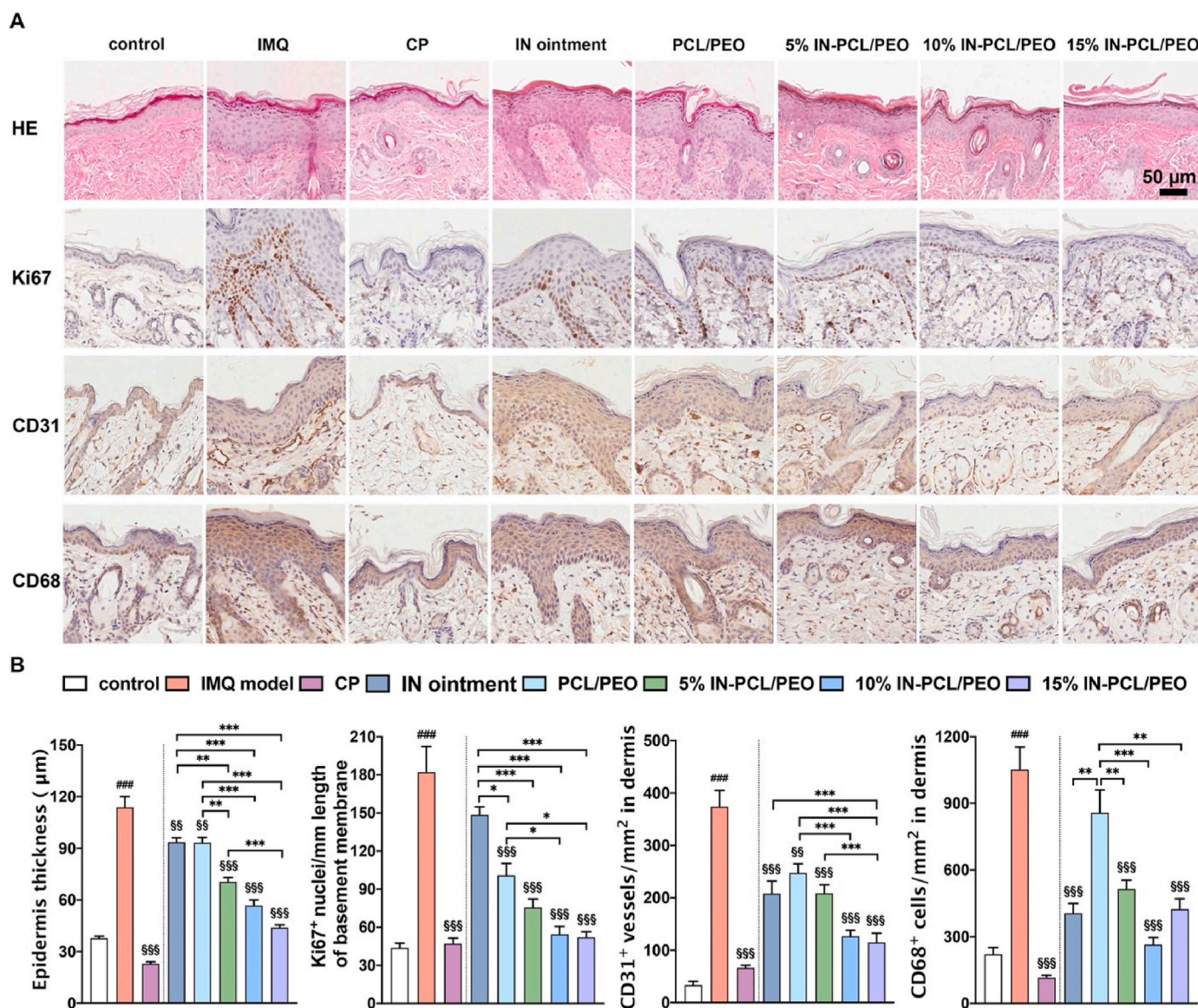

Fig. 5. Pathological analyses of dorsal skin in response to IN-PCL/PEO nanopatches in IMQ-induced psoriasis. (A) H&E staining, the expression of Ki67, CD31 and CD68 of the dorsal skin of psoriatic mice treated with indicated formulations. Scale bar: 50 μm. (B) Quantitative analyses of epidermal thickness, Ki67-positive cells, CD31-positive cells, and CD68-labelled cells. Data are presented as the mean ± SEM. $^{###}p < 0.005$ compared with control without any drug treatment; $^{§§}p < 0.01$ and $^{§§§}p < 0.005$ compared with IMQ; $^{*}p < 0.05$, $^{**}p < 0.01$, and $^{***}p < 0.005$ between treatments as indicated.

distinction between IN ointment and nanopatches. Additionally, pathological investigations of the liver, kidney and spleen confirmed the safety of the IN-PCL/PEO nanopatches (Fig. S6). Thus, our pathological assessment clarified a general anti-inflammatory potency of IN in IMQ-induced model of psoriasis and pinpointed that the advantage of IN-PCL/PEO nanopatches over IN ointment in psoriatic skin was mostly evident in cell proliferation and angiogenesis.

3.7. Ex-vivo drug permeation and retention of IN-PCL/PEO nanopatch

Drug permeation through scaly psoriasis lesions and its subsequent retention in the deeper dermis are key determinants for effective psoriasis topical treatment [46,47]. Because *in vivo* studies of medication absorption based on human skin tissues are impractical due to ethical concerns, *ex vivo* psoriatic skin of mice was utilized to assess the drug penetration and retention (Fig. 6). Using Franz diffusion cells, indigo was found exclusively in the epidermal layer, but not the dermis, of psoriatic skin, regardless of treatment of IN ointment or IN-PCL/PEO nanopatches. Intriguingly, we observed a dramatic reduction of epidermal indigo when exposed to IN-PCL/PEO nanopatches (1.4 ± 1.0 ng/cm^2) compared to indigo in the epidermal layer of IN ointment-treated skin (17.4 ± 7.3 ng/cm^2).

Since indigo is the component that gives IN its dark blue hue, this could explain why psoriatic skin exposed to IN ointment was heavily colored with dark blue. Compared to indigo, the overall retention of indirubin was more pronounced. Specifically, indirubin levels were substantially greater in both epidermis (64 ± 15.1 ng/cm^2) and dermis (68.3 ± 20.1 ng/cm^2) of psoriatic skin in IN-PCL/PEO-treated circumstances than in IN ointment (epidermis: 17.4 ± 7.3 ng/cm^2; and dermis: non-detected). Much the same as indirubin, the application of nanopatches resulted in twice the quantity of tryptanthrin retention in the epidermal layer (10.4 ± 2.5 ng/cm^2) relative to IN ointment (4.7 ± 1.9 ng/cm^2), although no difference in the amount of dermal tryptanthrin was detected between IN ointment and nanopatches. More crucially, we did not detect any signals of indigo, indirubin and tryptanthrin on the other side of the tested skin during the 30-min application period, suggesting a low probability of IN absorption into systemic circulation, which could lead to deleterious effects. Collectively, in comparison with IN ointment, IN-PCL/PEO nanopatches have a higher indirubin penetration in both epidermis and dermis, more tryptanthrin in epidermis, and less dark blue indigo accumulation in epidermis of psoriatic skin, indicating that the former two components may substantially contribute to the anti-psoriasis effectiveness of nanopatches.

These results highlight the importance of the electrospun membrane as the drug transdermal delivery system. Firstly, drugs in the formulation of traditional ointment are in the range of micrometers, while applications of electrospinning ensured an amorphous drug-loading in nano-scale fibers. This is critical for skin penetrations of drugs. Secondly, electrospun nanofibers have a relatively higher surface area volume ratio, which renders a larger drug-loading capacity than traditional ointments or patches. Thirdly, the mechanical properties of drug-loaded nanofibrous membranes prepared are suitable for skin application. Once applied to the skin and hydrated by the surrounding aqueous solution, nanofibrous membranes could adhere tightly to the skin, followed by an immediate drug release. Since electrospun nanofibers have a larger drug-loading capacity, the relative release of drug molecules is potentially improved. Then, with the amorphous dispersion of drug molecules from electrospun nanofibers and the highly increased release surface area by nanosized effect, the penetration or absorption of drugs through intercellular, intracellular, and transappendageal routes is further boosted, contributing to incremented retention of the drug in skin structures.

3.8. In vitro inhibition of proliferation and angiogenesis by major components of IN

Indirubin and tryptanthrin were the principal ingredients released from nanopatches (Fig. 3) and successfully delivered across psoriatic skin barriers (Fig. 6), suggesting that both indirubin and tryptanthrin are the effective components responsible for the therapeutic effect of IN. To verify this hypothesis, we first determined the cytotoxicity of indigo, indirubin and tryptanthrin in HaCat cells before testing their inhibitory efficiency in cell proliferation (Fig. S7). Using EGF at 10 ng/mL as a positive control (Fig. S8), all tested drugs inhibited EGF-induced cell proliferation in a dose-dependent manner (Fig. 7A). Among them, indigo and indirubin decreased maximum HaCat growth by 22.9% and 23.8%, respectively, and tryptanthrin suppressed cell growth by up to 64.5% when compared with positive controls, indicating that tryptanthrin was the most important component that restricted cell proliferation.

We then examined cell cycle progression. The fragmentation of DNA, which was detected as a sharp and discrete peak of G0/G1 cell population, represents apoptotic cells in flow cytometry. Compared to EGF-treated positive control cells that were halted at G0/G1 phase (Fig. 7B), indirubin and tryptanthrin significantly increased cell accumulation in G0/G1 phase by 11.6% and 14.5%, respectively, while decreasing S phase by 9.8% and 12% (Fig. 7C). By contrast, when cells were exposed to indigo, no significant effect was detected in cell cycle progression. To quantitatively interpret the result of cell apoptosis, we additionally performed an Annexin V-FITC/PI staining assay. As illustrated in Fig. 7D, there were fewer early (Annexin$^+$/PI$^-$) and late apoptotic (Annexin$^+$/PI$^+$) cells in EGF-treated cells compared to controls, verifying that EGF was an effective anti-apoptotic agent. Exposure
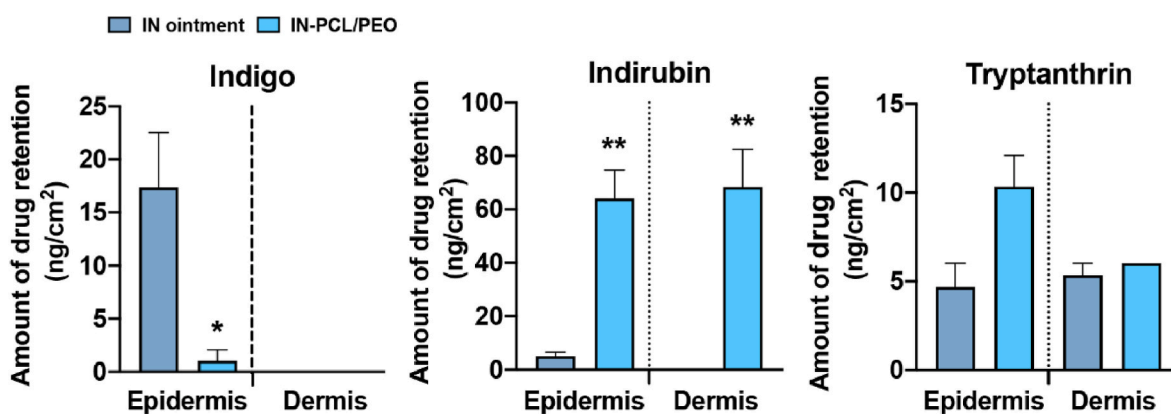

Fig. 6. Amounts of drug retention (ng/cm^2) in epidermal and dermal layers of psoriatic skin. The retention of indigo, indirubin and tryptanthrin in epidermal and dermal layers of psoriatic skin was evaluated by HPLC after 30 min treatment with either IN ointment or IN-PCL/PEO nanofibers using Franz diffusion cells. Data are presented as the mean $\pm$ SEM (n = 3). *$p < 0.05$ and **$p < 0.01$ compared with IN ointment.
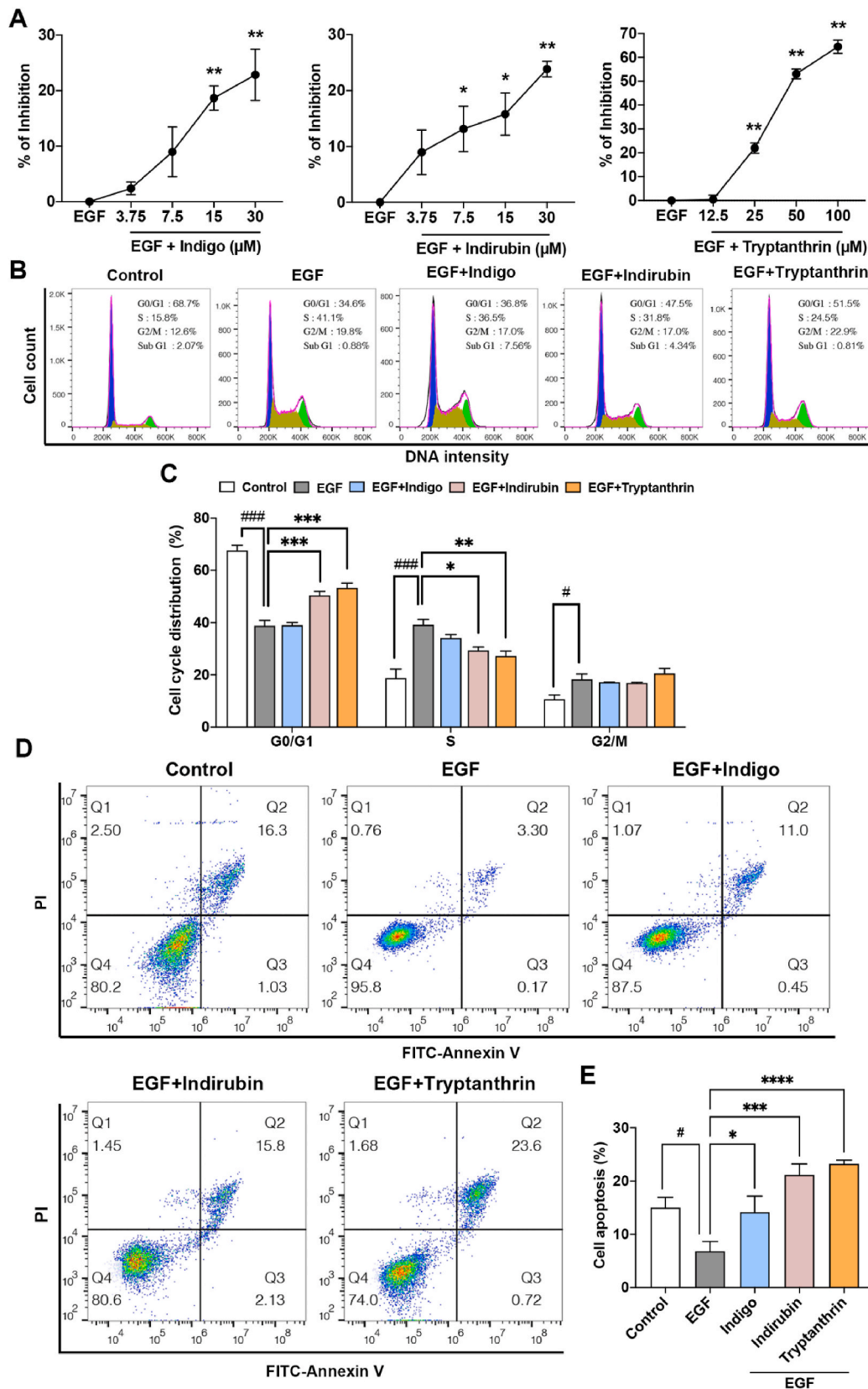
Fig. 7. Effects of major IN active components on cell proliferation, cell-cycle arrest, and apoptosis. (A) Inhibitory effects of indigo, indirubin and tryptanthrin on EGF-induced cell proliferation. (B) Determination of HaCat cell cycle in response to indigo, indirubin and tryptanthrin by flow cytometry analysis. (C) Effects of indigo, indirubin and tryptanthrin on cell cycle phase distribution of HaCat cells. (D and E) Apoptosis of HaCat cells in response to indicated treatments, as detected by flow cytometry analysis with FITC Annexin V/PI staining (D) followed by quantifications (E). (D) Q1: AV⁻/PI⁺, necrotic cells; Q2: AV⁺/PI⁺, late apoptotic cells; Q3: AV⁺/PI⁻, early apoptotic cells, and Q4: AV⁻/PI⁻, living cells. (A, C and E) Data are presented as the mean $\pm$ SEM. $^{\#}p < 0.05$ and $^{\#\#\#}p < 0.005$ relative to control; $^{*}p < 0.05$, $^{**}p < 0.01$, $^{***}p < 0.005$, and $^{****}p < 0.001$ relative to EGF treatment alone.

to indigo, indirubin and tryptanthrin significantly enhanced the early apoptosis from 0.17% in EGF to 0.45%, 2.13% and 0.72%, respectively, as well as late apoptosis from 3.30% in EGF to 11.0%, 15.8% and 23.6% (Fig. 7D). These findings clearly demonstrated that all three tested components, particularly indirubin and tryptanthrin, could induce cell death in EGF-treated HaCat cells (Fig. 7E). In sum, by arresting cells at G0/G1 phase and promoting cell apoptosis, both indirubin and tryptanthrin contributed significantly to the anti-proliferation activities of IN.

Considering that the maturation of migrated endothelial cells into a capillary tube is a critical step during angiogenesis [48], the potential effects of IN components on the early tube formation were further examined using three-dimensional Matrigel assays. Based on the safety profiles of indigo (3.75–30 μM), indirubin (3.75–30 μM) and tryptanthrin (12.5–100 μM) on HUVEC (Fig. S9), tube formation analysis was carried out in the presence of 50 ng/mL bFGF, which induced a massive network of well-branched tubes after 6 h (Fig. S10). In terms of vessel density, total junctions and total tube length, a general disruption of tube formation was observed in HUVEC treated with indigo, indirubin and tryptanthrin in a dose-dependent manner, albeit to varying degrees (Fig. 8A). The most powerful inhibition was observed in cells exposed to tryptanthrin, followed by indigo (Fig. 8B). Because capillary tube formation occurs mostly in the dermis, but we found minimal indigo retention in this layer of psoriatic skin (Fig. 6); hence, this set of data was suggestive of tryptanthrin as the principal suppressor of angiogenesis.

Taken together, we provided evidence that both indirubin and tryptanthrin, which were delivered more efficiently to epidermal and dermal layers of psoriatic skin by nanopatches (Fig. 6), played a decisive role by suppressing cell proliferation and angiogenesis, consistent with the better recovery of IMQ-induced psoriatic skin in mice treated with

IN-PCL/PEO nanopatches relative to IN ointment. Indigo, which caused unwanted skin coloration while providing modest therapeutic effects in cell proliferation and angiogenesis, was greatly reduced during IN nanopatch-based transdermal administration.

3.9. Effects of IN-PCL/PEO nanopatch on human psoriatic skin

To further evaluate the feasibility of topical applications of IN-PCL/PEO nanopatch on human skin and to assess therapeutic effects of IN in the PCL/PEO electrospun nanofiber system, we preliminarily enrolled three psoriasis patients. In the administration of IN-PCL/PEO nanopatches, a direct contact of IN-PCL/PEO nanopatches with psoriatic lesions simply required a few drops of water (Fig. 9A). Then, the IN-PCL/PEO nanopatches dried in 30 min and could be easily removed. The baseline psoriatic lesions and related changes in the shape/size of psoriatic plaques, the degree of scales and the redness of lesions were photographed over a 4-week period (Fig. 9B). Using the PASI score, a reduction in the redness and scales was obtained after 2 weeks of application, with a noteworthy alleviation in erythema, infiltration and scaling at the end of the 4-week treatment (Fig. 9C). There was no regional irritation or discomfort reported over the entire treatment period, and no traces of dark stains on the skin or clothes were recorded. Thus, this simple-to-apply nanopatch significantly reduced psoriatic lesions and may have increased patients compliance, indicating a promising bench-to-bedside translation of IN-PCL/PEO nanopatch in the management of psoriasis.

4. Conclusions

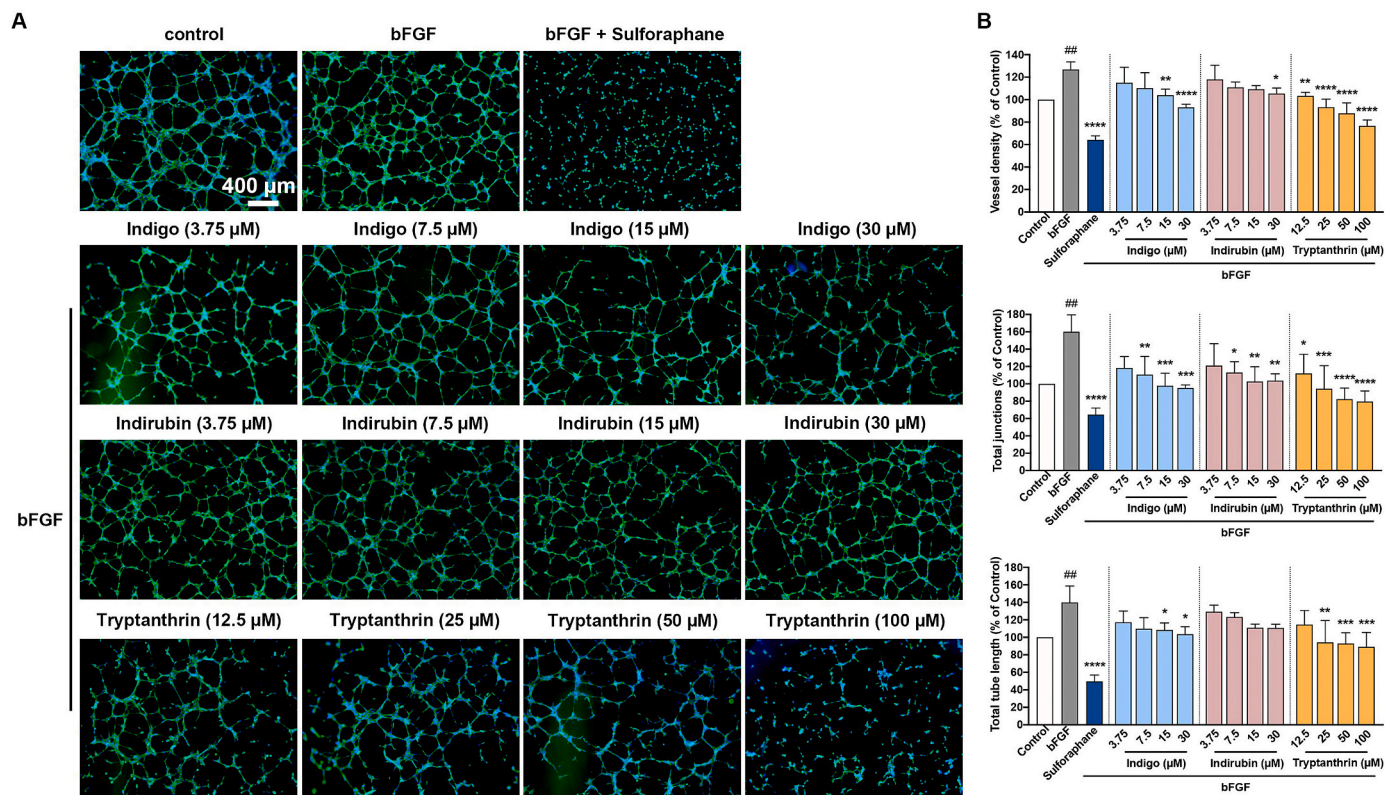In the current study, we aimed to fabricate a nanopatch loaded with

Fig. 8. Effects of major IN active components on HUVEC angiogenesis *in vitro*. (A) HUVEC tube formation was induced by bFGF, and fluorescently visualized after the exposure to indigo (3.75 μM, 7.5 μM, 15 μM and 30 μM), indirubin (3.75 μM, 7.5 μM, 15 μM and 30 μM), and tryptanthrin (12.5 μM, 25 μM, 50 μM and 100 μM) in comparison with positive control sulforaphane. Scale bar: 400 μm. (B) Vessel density (percentage covered area by vessel), total number of junctions and total vessel length were measured. Data were calculated and normalized to that of control (mean ± SEM, n = 3; $^{##}p < 0.01$ compared with control; $^{*}p < 0.05$, $^{**}p < 0.01$, $^{***}p < 0.005$, and $^{****}p < 0.001$ compared with bFGF).
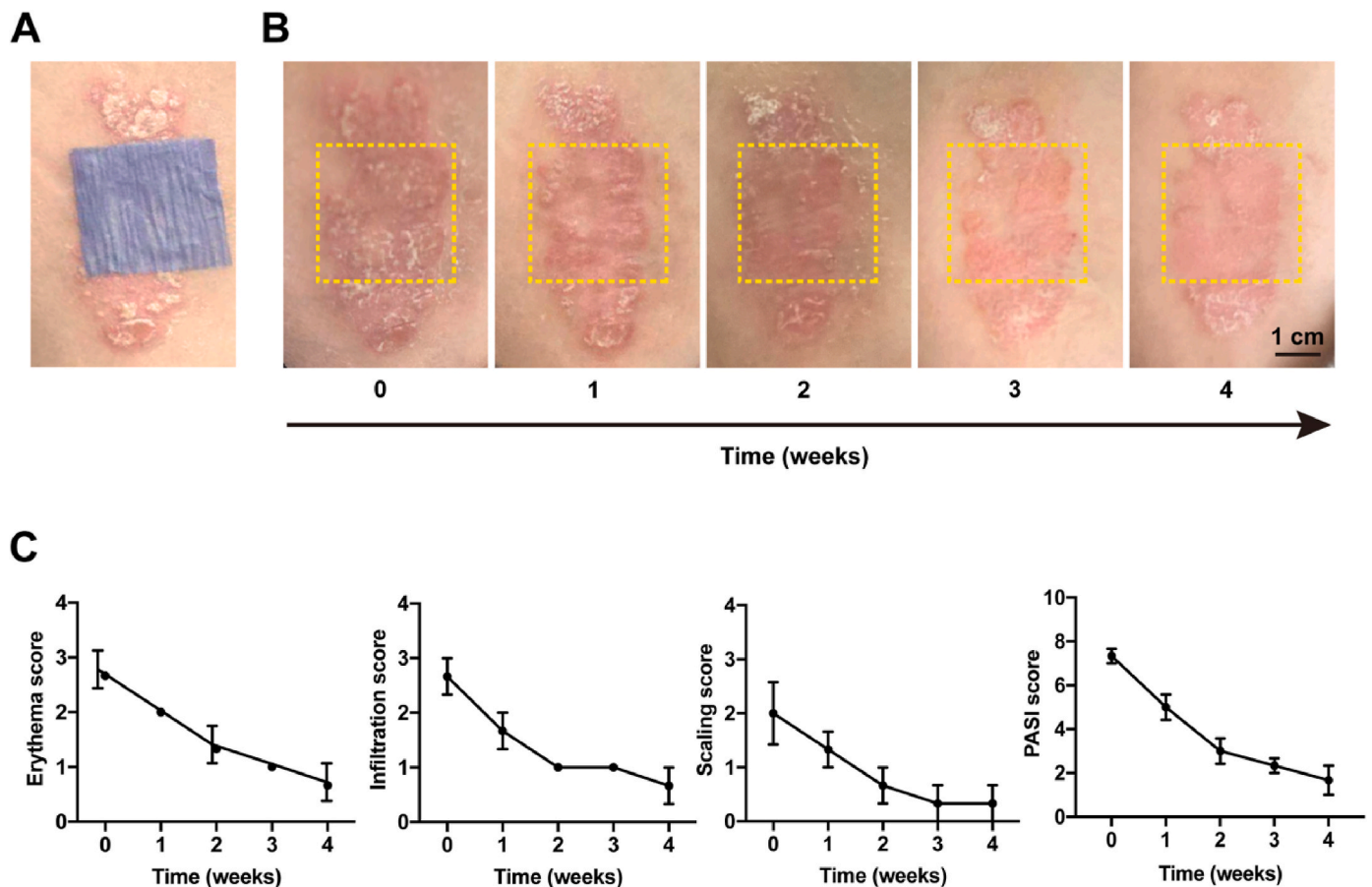
Fig. 9. Clinical observations of IN-PCL/PEO nanopatch on patients with vulgaris psoriasis. (A) Image of a 9 cm^2 IN-PCL/PEO nanopatch resting on the psoriatic skin of left forearm of a 32-year-old male patient with a psoriasis vulgaris lesion. (B) Topical application of IN-PCL/PEO nanopatch to the same the psoriatic lesion in (A) twice *per* day for 4 consecutive weeks. The yellow dashed box represents the region where IN-PCL/PEO nanopatch was topically applied. Scale bar: 1 cm. (C) Evaluations of erythema, infiltration, scaling and total PASI of psoriatic lesions of three evaluated patients treated with IN-PCL/PEO nanopatches. (For interpretation of the references to colour in this figure legend, the reader is referred to the Web version of this article.)

IN by combining blending electrospinning. The electrospun fibrous membranes produced are bead-free, continuous, and morphologically smooth, with excellent amphiphilic characteristics. Indigo, indirubin and tryptanthrin were identified and released from IN-PCL/PEO nanopatches as the primary active IN components. IN-PCL/PEO nanopatches demonstrated high efficacy in moderating psoriatic phenotypes without any signs of unfavorable lesional coloration, as compared to IN ointment by altering drug penetration and retention patterns of IN. As a result, the electrospinning-based nanotechnology opens up new opportunities for traditional medicinal herbs as topical therapies for psoriasis.

Credit author statement

RX, NL and PS: Conceptualization, Supervision, Methodology. PW, JG, SG, HL, CC, SH, YS, CW: Investigation, Validation, Data curation, Visualization. RX, NL, PW, JG: Writing – original draft preparation. NL, RX, WX: Writing-Reviewing and Editing. NL, RX: Funding acquisition. All authors contributed and approved the submitted version.

Declaration of competing interest

The authors declare no competing financial interests or non-financial interests.

Data availability

Data will be made available on request.

Acknowledgements

Appendix A. Supplementary data

Supplementary data to this article can be found online at https://doi.org/10.1016/j.mtbio.2023.100756.

References

[1] K. Walter, Psoriasis, JAMA 327 (19) (2022) 1936.
[2] M.A. Lowes, M. Suarez-Farinas, J.G. Krueger, Immunology of psoriasis, Annu. Rev. Immunol. 32 (2014) 227–255.
[3] F.O. Nestle, D.H. Kaplan, J. Barker, Mechanisms of disease: psoriasis, N. Engl. J. Med. 361 (5) (2009) 496–509.
[4] C.E.M. Griffiths, A.W. Armstrong, J.E. Gudjonsson, J. Barker, Psoriasis, Lancet 397 (10281) (2021) 1301–1315.
[5] J.E. Hawkes, T.C. Chan, J.G. Krueger, Psoriasis pathogenesis and the development of novel targeted immune therapies, J. Allergy Clin. Immunol. 140 (3) (2017) 645–653.
[6] R. Lande, E. Botti, C. Jandus, D. Dojcinovic, G. Fanelli, C. Conrad, G. Chamilos, L. Feldmeyer, B. Marinari, S. Chon, L. Vence, V. Riccieri, P. Guillaume, A. A. Navarini, P. Romero, A. Costanzo, E. Piccolella, M. Gilliet, L. Frasca, The

antimicrobial peptide LL37 is a T-cell autoantigen in psoriasis, Nat. Commun. 5 (2014) 5621.

[7] L. Uva, D. Miguel, C. Pinheiro, J. Antunes, D. Cruz, J. Ferreira, P. Filipe, Mechanisms of action of topical corticosteroids in psoriasis, Int J Endocrinol 2012 (2012), 561018.

[8] R.M. Grossman, S. Chevret, J. Abi-Rached, F. Blanchet, L. Dubertret, Long-term safety of cyclosporine in the treatment of psoriasis, Arch. Dermatol. 132 (6) (1996) 623–629.

[9] U.F. Haustein, M. Rytter, Methotrexate in psoriasis: 26 years' experience with low-dose long-term treatment, J. Eur. Acad. Dermatol. Venereol. 14 (5) (2000) 382–388.

[10] J.J. Hong, E.K. Hadeler, M.L. Mosca, N.D. Brownstone, T. Bhutani, W.J. Liao, TNF-alpha inhibitors and ustekinumab for the treatment of psoriasis: therapeutic utility in the era of IL-17 and IL-23 inhibitors, J. Psoriasis Psoriatic Arthritis 7 (2) (2022) 79–92.

[11] A.W. Armstrong, C. Read, Pathophysiology, clinical presentation, and treatment of psoriasis: a review, JAMA 323 (19) (2020) 1945–1960.

[12] M. Naganuma, S. Sugimoto, K. Mitsuyama, T. Kobayashi, N. Yoshimura, H. Ohi, S. Tanaka, A. Andoh, N. Ohmiya, K. Saigusa, T. Yamamoto, Y. Morohoshi, H. Ichikawa, K. Matsuoka, T. Hisamatsu, K. Watanabe, S. Mizuno, W. Suda, M. Hattori, S. Fukuda, A. Hirayama, T. Abe, M. Watanabe, T. Hibi, Y. Suzuki, T. Kanai, I.S. Group, Efficacy of indigo naturalis in a multicenter randomized controlled trial of patients with ulcerative colitis, Gastroenterology 154 (4) (2018) 935–947.

[13] Y.K. Lin, L.C. See, Y.H. Huang, Y.C. Chang, T.C. Tsou, T.Y. Lin, N.L. Lin, Efficacy and safety of Indigo naturalis extract in oil (Lindioil) in treating nail psoriasis: a randomized, observer-blind, vehicle-controlled trial, Phytomedicine 21 (7) (2014) 1015–1020.

[14] R. Hoessel, S. Leclerc, J.A. Endicott, M.E. Nobel, A. Lawrie, P. Tunnah, M. Leost, E. Damiens, D. Marie, D. Marko, E. Niederberger, W. Tang, G. Eisenbrand, L. Meijer, Indirubin, the active constituent of a Chinese antileukaemia medicine, inhibits cyclin-dependent kinases, Nat. Cell Biol. 1 (1) (1999) 60–67.

[15] A.V. Schwaiberger, E.H. Heiss, M. Cabaravdic, T. Oberan, J. Zaujec, D. Schachner, P. Uhrin, A.G. Atanasov, J.M. Breuss, B.R. Binder, V.M. Dirsch, Indirubin-3'-monoxime blocks vascular smooth muscle cell proliferation by inhibition of signal transducer and activator of transcription 3 signaling and reduces neointima formation in vivo, Arterioscler. Thromb. Vasc. Biol. 30 (12) (2010) 2475–2481.

[16] N. Liu, G.X. Zhang, Y.T. Niu, Q. Wang, J. Zheng, J.M. Yang, T. Sun, J.G. Niu, J. Q. Yu, Anti-inflammatory and analgesic activities of indigo through regulating the IKKbeta/IkappaB/NF-kappaB pathway in mice, Food Funct. 11 (10) (2020) 8537–8546.

[17] P.P. Bandekar, K.A. Roopnarine, V.J. Parekh, T.R. Mitchell, M.J. Novak, R. R. Sinden, Antimicrobial activity of tryptanthrins in Escherichia coli, J. Med. Chem. 53 (9) (2010) 3558–3565.

[18] H.L. Chan, H.Y. Yip, N.K. Mak, K.N. Leung, Modulatory effects and action mechanisms of tryptanthrin on murine myeloid leukemia cells, Cell. Mol. Immunol. 6 (5) (2009) 335–342.

[19] Y.K. Lin, W.R. Wong, Y.C. Chang, C.J. Chang, P.K. Tsay, S.C. Chang, J.H. Pang, The efficacy and safety of topically applied indigo naturalis ointment in patients with plaque-type psoriasis, Dermatology 214 (2) (2007) 155–161.

[20] Y.K. Lin, W.R. Wong, J.H. Su Pang, Successful treatment of recalcitrant psoriasis with Indigo naturalis ointment, Clin. Exp. Dermatol. 32 (1) (2007) 99–100.

[21] Y.K. Lin, C.J. Chang, Y.C. Chang, W.R. Wong, S.C. Chang, J.H. Pang, Clinical assessment of patients with recalcitrant psoriasis in a randomized, observer-blind, vehicle-controlled trial using indigo naturalis, Arch. Dermatol. 144 (11) (2008) 1457–1464.

[22] Y.K. Lin, L.C. See, Y.H. Huang, Y.C. Chang, T.C. Tsou, Y.L. Leu, Y.M. Shen, Comparison of refined and crude indigo naturalis ointment in treating psoriasis: randomized, observer-blind, controlled, intrapatient trial, Arch. Dermatol. 148 (3) (2012) 397–400.

[23] Y.K. Lin, Indigo naturalis oil extract drops in the treatment of moderate to severe nail psoriasis: a small case series, Arch. Dermatol. 147 (5) (2011) 627–629.

[24] Y.K. Lin, Y.C. Chang, R.C. Hui, L.C. See, C.J. Chang, C.H. Yang, Y.H. Huang, A Chinese herb, indigo naturalis, extracted in oil (lindioil) used topically to treat psoriatic nails: a randomized clinical trial, JAMA Dermatol 151 (6) (2015) 672–674.

[25] Y.K. Lin, L.C. See, Y.H. Huang, C.C. Chi, R.C. Hui, Comparison of indirubin concentrations in indigo naturalis ointment for psoriasis treatment: a randomized, double-blind, dosage-controlled trial, Br. J. Dermatol. 178 (1) (2018) 124–131.

[26] Y. Zhang, M. Zhang, D. Cheng, S. Xu, C. Du, L. Xie, W. Zhao, Applications of electrospun scaffolds with enlarged pores in tissue engineering, Biomater. Sci. 10 (6) (2022) 1423–1447.

[27] X.R. Xie, Y.J. Chen, X.Y. Wang, X.Q. Xu, Y.H. Shen, A.U.R. Khan, A. Aldalbahi, A. E. Fetz, G.L. Bowlin, M. El-Newehy, X.M. Mo, Electrospinning nanofiber scaffolds for soft and hard tissue regeneration, J. Mater. Sci. Technol. 59 (2020) 243–261.

[28] C. Gao, L. Zhang, J. Wang, M. Jin, Q. Tang, Z. Chen, Y. Cheng, R. Yang, G. Zhao, Electrospun nanofibers promote wound healing: theories, techniques, and perspectives, J. Mater. Chem. B 9 (14) (2021) 3106–3130.

[29] A.S. Arampatzis, K.N. Kontogiannopoulos, K. Theodoridis, E. Aggelidou, A. Rat, A. Willems, I. Tsivintzelis, V.P. Papageorgiou, A. Kritis, A.N. Assimopoulou, Electrospun wound dressings containing bioactive natural products: physico-chemical characterization and biological assessment, Biomater. Res. 25 (1) (2021) 23.

[30] R. Goyal, L.K. Macri, H.M. Kaplan, J. Kohn, Nanoparticles and nanofibers for topical drug delivery, J. Contr. Release 240 (2016) 77–92.

[31] F.F. Sahle, T. Gebre-Mariam, B. Dobner, J. Wohlrab, R.H. Neubert, Skin diseases associated with the depletion of stratum corneum lipids and stratum corneum lipid substitution therapy, Skin Pharmacol. Physiol. 28 (1) (2015) 42–55.

[32] S. Knox, N.M. O'Boyle, Skin lipids in health and disease: a review, Chem. Phys. Lipids 236 (2021), 105055.

[33] T.K. Dash, V.B. Konkimalla, Poly-small je, Ukrainian-caprolactone based formulations for drug delivery and tissue engineering: a review, J. Contr. Release 158 (1) (2012) 15–33.

[34] M. Gumusderelioglu, S. Dalkiranoglu, R.S.T. Aydin, S. Cakmak, A novel dermal substitute based on biofunctionalized electrospun PCL nanofibrous matrix, J. Biomed. Mater. Res. 98a (3) (2011) 461–472.

[35] Y.F. Li, M. Rubert, H. Aslan, Y. Yu, K.A. Howard, M. Dong, F. Besenbacher, M. Chen, Ultraporous interweaving electrospun microfibers from PCL-PEO binary blends and their inflammatory responses, Nanoscale 6 (6) (2014) 3392–3402.

[36] S.M. Garg, I.M. Paiva, M.R. Vakili, R. Soudy, K. Agopsowicz, A.H. Soleimani, M. Hitt, K. Kaur, A. Lavasanifar, Traceable PEO-poly(ester) micelles for breast cancer targeting: the effect of core structure and targeting peptide on micellar tumor accumulation, Biomaterials 144 (2017) 17–29.

[37] F. Asghari, D. Rabiei Faradonbeh, Z.V. Malekshahi, H. Nekounam, B. Ghaemi, Y. Yousefpoor, H. Ghanbari, R. Faridi-Majidi, Hybrid PCL/chitosan-PEO nanofibrous scaffolds incorporated with A. euchroma extract for skin tissue engineering application, Carbohydr. Polym. 278 (2022), 118926.

[38] L. Hou, X. Zhang, P.E. Mikael, L. Lin, W. Dong, Y. Zheng, T.J. Simmons, F. Zhang, R.J. Linhardt, Biodegradable and bioactive PCL-PGS core-shell fibers for tissue engineering, ACS Omega 2 (10) (2017) 6321–6328.

[39] S. Thatikonda, V. Pooladanda, D.K. Sigalapalli, C. Godugu, Piperlongumine regulates epigenetic modulation and alleviates psoriasis-like skin inflammation via inhibition of hyperproliferation and inflammation, Cell Death Dis. 11 (1) (2020) 21.

[40] E. Zudaire, L. Gambardella, C. Kurcz, S. Vermeren, A computational tool for quantitative analysis of vascular networks, PLoS One 6 (11) (2011), e27385.

[41] B.C. Liau, T.T. Jong, M.R. Lee, S.S. Chen, LC-APCI-MS method for detection and analysis of tryptanthrin, indigo, and indirubin in daqingye and banlangen, J. Pharm. Biomed. Anal. 43 (1) (2007) 346–351.

[42] B. Darbasizadeh, S.A. Mortazavi, F. Kobarfard, M.R. Jaafari, A. Hashemi, H. Farhadnejad, B. Feyzi-barnaji, Electrospun Doxorubicin-loaded PEO/PCL core/sheath nanofibers for chemopreventive action against breast cancer cells, J. Drug Deliv. Sci. Technol. (2021) 64.

[43] X. Zhou, Y. Chen, L. Cui, Y. Shi, C. Guo, Advances in the pathogenesis of psoriasis: from keratinocyte perspective, Cell Death Dis. 13 (1) (2022) 81.

[44] R. Heidenreich, M. Rocken, K. Ghoreschi, Angiogenesis drives psoriasis pathogenesis, Int. J. Exp. Pathol. 90 (3) (2009) 232–248.

[45] D. Creamer, D. Sullivan, R. Bicknell, J. Barker, Angiogenesis in psoriasis, Angiogenesis 5 (4) (2002) 231–236.

[46] P. Bhardwaj, P. Tripathi, S. Pandey, R. Gupta, R.K. Khar, P.R. Patil, Improved dermal delivery of pentoxifylline niosomes for the management of psoriasis: development, optimization and in-vivo studies in imiquimod induced psoriatic plaque model, J. Drug Deliv. Sci. Technol. (2022) 75.

[47] T. Fukuta, D. Tanaka, S. Inoue, K. Michiue, K. Kogure, Overcoming thickened pathological skin in psoriasis via iontophoresis combined with tight junction-opening peptide AT1002 for intradermal delivery of NF-kappaB decoy oligodeoxynucleotide, Int. J. Pharm. 602 (2021), 120601.

[48] L. Lamalice, F. Le Boeuf, J. Huot, Endothelial cell migration during angiogenesis, Circ. Res. 100 (6) (2007) 782–794.